CAPABILITIES OF WIND TUNNELS WITH TWO ADAPTIVE WALLS TO MINIMIZE BOUNDARY INTERFERENCE IN 3-D MODEL TESTING*

Rainer Rebstock and Edwin E. Lee, Jr.
Experimental Techniques Branch
NASA Langley Research Center
Hampton, VA

SUMMARY

An initial wind tunnel test was made to validate a new wall adaptation method for 3-D models in test sections with two adaptive walls. The model tested was an unswept semi-span wing. It was mounted on one sidewall of NASA's 0.3-m Transonic Cryogenic Tunnel, which is fitted with flexible top and bottom walls (semispan/tunnel height = 0.51). The vertical position of the wing in the test section could be changed to increase the wall interference. The experiments were conducted at freestream Mach numbers of 0.7, 0.8 and 0.85 and model angles-of-attack between 0 and 7°. Model forces and moments were measured with a five-component balance.

First part of the adaptation strategy is an on-line assessment of wall interference at the model position. The wall-induced blockage was very small at all test conditions. Noticeable lift interference occurred at higher angles of attack with the walls set aerodynamically straight. The induced upwash varied considerably in the chordwise as well as in the spanwise direction.

The adaptation of the top and bottom tunnel walls is aimed at achieving a correctable flow condition. The deflections are calculated to exactly eliminate the upwash gradient and the blockage velocity along one straight line in the test section. The location of this target line can be chosen with respect to the actual interference at the model.

The blockage was virtually zero throughout the wing planform after the wall adjustment. The upwash velocity was small and nearly constant in chordwise direction. However, a spanwise gradient remained, even after a second wall adaptation. The induced angle of attack at the mean aerodynamic chord of the wing was chosen as correction to the freestream velocity vector.

The lift curve measured with the walls adapted agreed very well with interference free-data for $M_\infty = 0.7$, regardless of the vertical position of the wing in the test section. However, noticeable discrepancies remained at $M_\infty = 0.85$ and high model angles of attack. This deviation was probably caused by an inaccurate wall interference assessment due to an insufficient number of pressure readings at the tunnel boundary.

The 2-D wall adaptation can significantly improve the correctability of 3-D model data. Nevertheless, residual spanwise variations of wall interference are inevitable. This may restrict the usable model span. Further tests with different configurations are needed to clarify this point.

---

*This work was done while the first author held a National Research Council - NASA Research Associateship

INTRODUCTION

Wall interference can be eliminated by adjusting the flow at the test section boundary. The idea is to provide a streamtube that is the same as in free-air.

This concept is relatively easy to apply in 2-D airfoil testing. Only the top and bottom walls of the test section need to be flexible or ventilated. The side walls can be solid. A practical algorithm for streamlining the walls was devised by Sears in 1973 (ref. 1). Effectively interference-free data have been obtained in these "2-D adaptive" test sections for both conventional and supercritical airfoils. References 2, 3, 4 and 5 provide more details.

The use of adaptive walls is less obvious for testing 3-D models. A simulation of free-air conditions requires active flow control along the whole test section boundary. The three facilities built so far therefore almost inevitably suffer from increased mechanical and operational complexity (refs. 3 and 4).

A simpler approach for transonic 3-D testing has been outlined by Kemp (ref. 6). His idea is to provide only the amount of wall control necessary to achieve a correctable flow condition. An on-line interference assessment method would be used to categorize the disturbances at the model as negligible, correctable or uncorrectable according to the required data accuracy.

The practical implications of this concept were independently studied by Harney and Wedemeyer. Harney shows experimentally that a 2-D wall adaptation has the potential to substantially reduce the interference velocities in the region of the tested model (ref. 7). In other words, a 2-D adaptive-wall test section may also be adequate for testing 3-D models.

Wedemeyer develops a wall adaptation technique for this purpose (ref. 8). Assuming linear potential flow, he calculates wall deflections that would lead to interference-free flow at the tunnel centerline. (The method is also applicable, in principle, if the top and bottom walls of the test section are ventilated rather than flexible.) The interference velocities (blockage and upwash) are deduced from the slope of the two flexible walls and their centerline pressure distributions. No explicit information about the tested model is needed.

A computer program of the adaptation method was developed in cooperation with Lamarche (refs. 9 and 10). Wind tunnel experiments at TU Berlin and ONERA/CERT demonstrated the soundness of this concept. References 3 and 10 contain a detailed analysis of the test results.

The Wedemeyer-Lamarche technique uses the same few wall pressure measurements as in airfoil testing. This makes it easy to apply, but seems to preclude an accurate interference assessment, at least in half-model tests. Consequently, no "figure-of-merit" has been defined (see ref. 4). The convergence of the wall adjustments is the only criterion to estimate the progress of the adaptation. This may lead to more iterations than necessary to achieve a correctable condition. Moreover, a separate method is needed to determine the residual interference at the model (ref. 11).

In this paper, an improved wall adaptation strategy for 3-D models in 2-D adaptive wind tunnels is described. Its essential features are:

(1) accurate on-line wall interference assessment based on flow measurements at the tunnel boundary ("two-variable method")
(2) elimination of wall interference at a user defined straight line in the test section
(3) evaluation of residual interference in terms of a Mach number and angle-of-attack correction

Initial validation tests have been performed with a semi-span wing in NASA Langley's 0.3-m TCT with flexible top and bottom walls. The model forces measured with the tunnel walls adapted are generally in good agreement with interference-free values.

ASSESSMENT OF WALL INTERFERENCE

Wall interference in the test section is deduced from the pressure distribution and the no-flux condition at the four test section walls (or equivalent measurements). A representation of the tested model is not required. Reference 12 provides a detailed description of the technique. The essential steps are as follows:

The disturbance velocities induced by the tunnel boundary are assumed to be small and irrotational. Their potential ϕ_W fulfills the linear differential equation

$$\beta^2\partial^2\phi_W/\partial X_P^2 + \partial^2\phi_W/\partial Y_P^2 + \partial^2\phi_W/\partial Z_P^2 = 0 \qquad (1)$$

$$\beta = (1-M_\infty^2)^{1/2}$$

throughout the test section as long as the flow around the model is dominantly subcritical.

We seek a solution of (1) in form of a source potential

$$\phi_W(P) = -1/4\pi\int_S \sigma_W(Q)g(P,Q)dQ$$

with

$$g(P,Q) = \{(X_P-X_Q)^2+\beta^2(Y_P-Y_Q)^2+\beta^2(Z_P-Z_Q)^2\}^{-1/2} \qquad (2)$$

The sources $\sigma_W(Q)$ are distributed at a control surface S enclosing the model. We choose the cylindrical streamtube formed by the non-deflected test section walls.

Equation 2 represents the wall constraint as a source-sink distribution. The goal is to determine the local strength $\sigma_W(Q)$ from the flow condition at the tunnel boundary.

The measured wall pressures are first transformed into axial disturbance velocities u_I and the local wall slope into disturbance velocities v_I normal to the control surface S. The number of pressure measurements should be large enough to allow a precise interpolation both in streamwise and cross-stream direction (see APPARATUS).

The following analysis is a direct application of Sears' adaptive wall concept (refs. 1 and 4). The essential idea is to extend the experimental flow field in the

test section to infinity by adding a computed exterior flow. This fictitious flow satisfies the appropriate (farfield) differential equations and the condition of vanishing disturbances at infinity. One of the two measured distributions, say u_I, serves as inner boundary condition. If the flow field in the test section is interference-free, it matches perfectly with the computed outer flow at the control surface. In this case, the combined flow fields simply represent the unconfined flow around the model. The computed (v_E) and measured v-distributions (and all other flow variables) are the same at the control surface.

However, if a mismatch occurs, $v_E - v_I \neq 0$ at S, the experimental flow field is not consistent with the farfield boundary conditions. Indeed, the discontinuity in the v-component completely defines the wall interference in the test section. We can see this as follows:

For subsonic freestream Mach numbers, the flow in the farfield fulfills the linearized potential equation (1). The exterior flow field computation thus becomes a Dirichlet problem for the infinite region beyond the tunnel boundary. We can construct the solution in terms of a source-sink distribution at the control surface. The resulting surface integral is similar to equation (2), but the field point P now lies in the exterior region. The potential generated within the test section has no physical significance.

$$\phi_E(P) = -1/4\pi \int_S \sigma_E(Q) g(P,Q) dQ \qquad (3)$$

The unknown singularity strength σ_E is uniquely defined by the inner boundary condition. In fact, streamwise integration of the prescribed u_I-distribution determines the potential at the control surface

$$\phi_E(P) = \int_{-\infty}^{X_P} u_I(T, Y_P, Z_P) dT \quad , \quad P \in S \qquad (4)$$

The integration upstream of the test section can usually be ignored in practice. However, an extrapolation of u_I in downstream direction is often required.

A combination of (3) and (4) leads to an integral equation of the first kind for σ_E. We can solve it by approximating the surface integral with a suitable quadrature formula.

Differentiation of the solution in normal direction finally yields the desired outer v-component v_E at S

$$v_E(P) = \partial\phi_E / \partial n_E(P) \quad , \quad P \in S \qquad (5)$$

If a jump in the normal velocity occurs, $v_E - v_I \neq 0$ at S, the experimental flow field is not interference-free. However, this discontinuity can be removed by putting sources and sinks at the control surface that exactly compensate the local flux imbalance. The required singularity strength is given by Gauss' flux theorem as

$$\sigma(P) = v_I(P) - v_E(P) \qquad (6)$$

The added singularities modify both the flow field in the test section and the computed exterior flow. The resulting flow field is continuous at the control surface and still fulfills the boundary condition of vanishing disturbances at

infinity. In other words, the modified flow field is interference-free. The source layer $\sigma(P)$ generates velocity perturbations within the test section that exactly cancel the wall interference.

Consequently, the singularity distribution that represents the tunnel walls is given by

$$\sigma_W(P) = - \sigma(P) = v_E(P) - v_I(P) \tag{7}$$

Insertion of (7) into (2) defines the wall interference potential everywhere in the test section. The wall-induced velocities follow by differentiation.

CALCULATION OF ADAPTED WALL SHAPES

A deflection of the top and bottom walls of the test section changes the blockage and upwash interference experienced by the model. The perturbations caused by small contour changes are governed by the linear potential equation

$$\beta^2 \phi_{XX} + \phi_{ZZ} = 0 \tag{8}$$

The cross-stream component is zero, since the wall deflections are constant across the tunnel width.

The existence of a flow potential allows us to calculate the induced velocities

$$\begin{aligned} u(X,Z) &= \phi_X(X,Z) \\ w(X,Z) &= \phi_Z(X,Z) \end{aligned} \tag{9}$$

everywhere in the test section.

An adjustment of the wall contours is, of course, aimed at minimizing the wall interference in the region of the tested model. The blockage and upwash velocities for the given wall shape are known from the wall interference potential (equation 2)

$$\begin{aligned} u_W(P) &= \partial\phi_W(P)/\partial X_P \\ w_W(P) &= \partial\phi_W(P)/\partial Z_P \end{aligned} \tag{10}$$

We disregard the cross-stream component since it cannot be reduced by a 2-D wall adaptation.

The physical condition for the wall adaptation therefore reads

$$\begin{aligned} (u + u_W)_{Model} &= \text{Min} \\ (w + w_W)_{Model} &= \text{Min} \end{aligned} \tag{11}$$

As we can see, the determination of the required deflections is an inverse problem. We need to simplify it in order to find a solution. A reasonable compromise is as follows:

We pick the vertical plane $Y = Y_0$ in the test section where the wall interference is worst. Within this plane we define a straight target line Z_0 = const. that passes through the model region.

An easy-to-impose boundary condition for the wall adaptation is

$$\begin{aligned} u(X,Z_0) + u_W(X,Y_0,Z_0) &= 0 \\ w(X,Z_0) + w_W(X,Y_0,Z_0) &= 0 \end{aligned} \tag{12}$$

In other words, it is feasible to exactly cancel the blockage and upwash interference along the target line. (However, it is often more practical to just eliminate the upwash-gradient and include the remaining constant value in the angle-of-attack correction. See RESULTS AND DISCUSSION.) The residual interference in the model region can be accounted for as corrections to the freestream velocity vector.

To find the desired deflections Δh_u (upper wall) and Δh_l (lower wall), we take advantage of the linearity of the potential equation (8). Basically, we expand Δh_u and Δh_l in Fourier series, calculate the induced disturbance velocities, and then determine the unknown series coefficients by imposing the boundary condition (12):

$$\begin{aligned} \Delta h_l(X) &= a_0 X + \sum_{n=1}^{\infty} a_n \sin(\lambda_n X) \\ \Delta h_u(X) &= c_0 X + \sum_{n=1}^{\infty} c_n \sin(\lambda_n X) \end{aligned} \tag{13}$$

$$\lambda_n = n\pi/L, \; L = \text{test section length}$$

The linear divergence terms are added to allow non-zero deflections at the test section end (allowance for model wake).

The calculation of the induced disturbance velocities is easier in terms of the stream function ψ rather than the potential ϕ. The two functions are related through the (Cauchy-Riemann) differential equations

$$\psi_\xi = -\phi'_\eta \; , \; \psi_\eta = \phi'_\xi \tag{14}$$

where $\phi'(\xi,\eta)$ denotes the incompressible potential obtained from the Prandtl-Glauert transformation

$$X = \xi \; , \; Z = \eta/\beta \; , \; \phi(X,Z) = \phi'(\xi,\eta)/\beta \tag{15}$$

The boundary-value problem for the stream function follows from (13), (14) and (15) as

$$\begin{aligned} \psi_{\xi\xi} + \psi_{\eta\eta} &= 0 \\ \psi(\xi,-\beta H/2) &= -\Delta h_l(\xi) \; , \; 0 \le \xi \le L \\ \psi(\xi,\beta H/2) &= -\Delta h_u(\xi) \; , \; 0 \le \xi \le L \end{aligned} \tag{16}$$

(H = test section height)

The solution consists of two parts

$$\psi(\xi,\eta) = \psi_1(\xi,\eta) + \psi_2(\xi,\eta)$$

$$\psi_1(\xi,\eta) = -\{(a_0+c_0)/2 + (c_0-a_0)\eta/\beta H\}\xi \qquad (17)$$

$$\psi_2(\xi,\eta) = \sum_{n=1}^{\infty}\{a_n\sinh[\lambda_n(\eta-\beta H/2)] - c_n\sinh[\lambda_n(\eta+\beta H/2)]\}\ \sin(\lambda_n\xi)/\sinh(\lambda_n\beta H)$$

ψ_1 represents the disturbances caused by a linear divergence of the top and bottom walls. The Fourier solution ψ_2 can be derived by a separation of the independent variables. Ref. 13 describes this technique in detail.

The velocities induced at the target line Z_0 = const., result from (9), (14) and (15)

$$u(X,Z_0) = \psi_\eta(\xi,\beta Z_0)/\beta$$

$$w(X,Z_0) = -\psi_\xi(\xi,\beta Z_0) \qquad (18)$$

We develop the upwash and blockage interference at the target line into Fourier series compatible with (18)

$$u_W(X) = u_W(L)X/L + \sum_{n=1}^{\infty} r_n\sin(\lambda_n X)$$

$$w_W(X) = s_0/2 + \sum_{n=1}^{\infty} s_n\cos(\lambda_n X) \qquad (19)$$

with the coefficients

$$r_n = 2/L \int_0^L \{u_W(X)-u_W(L)X/L\}\sin(\lambda_n X)dX\ ,\ n=1,2,...$$

$$s_n = 2/L \int_0^L w_W(X)\cos(\lambda_n X)dX\ ,\ n=0,1,... \qquad (20)$$

Imposition of the boundary condition (12) finally leads (after some straightforward calculations) to the following expressions for the series coefficients in (13)

$$a_0 = -s_0/2 - \beta^2 u_W(L)(H+2Z_0)/2L$$

$$a_n = -1/\lambda_n\ \{\beta r_n\sinh[\lambda_n\beta(Z_0+H/2)] + s_n\cosh[\lambda_n\beta(Z_0+H/2)]\}$$

$$c_0 = -s_0/2 + \beta^2 u_W(L)(H-2Z_0)/2L \qquad (21)$$

$$c_n = -1/\lambda_n\ \{\beta r_n\sinh[\lambda_n\beta(Z_0-H/2)] + s_n\cosh[\lambda_n\beta(Z_0-H/2)]\}$$

As we can see, the determination of the adapted wall shape involves three steps. First, computation of the Fourier coefficients r_n and s_n (eq. 20). Since the blockage and upwash velocities are very smooth, both sets of coefficients rapidly go

to zero with increasing frequency n. Typically, the lowest 8 to 12 frequencies provide enough resolution. We pick N = 16 (= 2^4) in order to apply the very efficient FFT-method. This requires an even distribution of the input values $u_w(X_i)$ and $w_w(X_i)$, i=1,...,N along the target line. Reference 14 provides more details on FFT and contains a suitable computer program. The subsequent evaluation of the algebraic equations (21) is straightforward. The coefficients a_n and c_n, n=0,...,N-1 determine the wall deflections (eq. 13). We can compute the finite sums (inverse Fourier transform) with the same FFT computer program as in step 1. All three steps combined require very little execution time, even on a small computer.

APPARATUS

We conducted the experiment in NASA Langley's 0.3-M Transonic Cryogenic Tunnel. An adaptive test section with flexible top and bottom walls was installed in the tunnel circuit in 1985. It is nominally 33cm (13 inches) square and has an effective length of 1.42m (55.8 inches). Reference 5 describes the facility in more detail.

The model was a scaled-up (1.6 times) replica of a semi-span wing tested at Langley Research Center in 1951 (ref. 15). It was selected for the experiment because of the essentially free-air data available from this test. We measured the forces and moments on the model with a five-component strain gauge balance. Figure 1 shows the apparatus in detail, including the model turntable, which was installed in the right sidewall of the test section. We could mount the wing at two vertical positions; the tunnel centerline and halfway between the center and the top wall. Figure 2 shows the wing in the center position.

The blockage ratio of the model in the TCT adaptive wall test section was 0.79% and the semi-span to tunnel width ratio was 0.51. Table 1 provides more information about the wing geometry and summarizes the test conditions. As in the early Langley test, all experiments were performed without a boundary-layer trip.

Recording of the static pressure distribution at the tunnel walls provided some difficulty. The test section was only equipped with pressure orifices at the centerline of the top- and bottom walls, which is adequate for airfoil testing. On the other hand, three rows of orifices above and below the model and one row at one sidewall are typically required for an accurate wall interference assessment in 3-D flows (ref. 16).

However, it was too time-consuming to add orifices on the flexible walls. Instead, we installed two rows at the right sidewall of the test section, as close to the flex walls as possible. The orifices drilled in the model turntable show the exact location of the two rows (see figure 1). Their displacement for non-zero angle-of-attack was ignored in the wall interference computations. The opposite sidewall was equipped with 14 pressure taps, concentrated in the model region.

The inaccurate representation of the wall pressure distribution is probably responsible for the noticeable residual interference at higher Mach numbers and angles-of-attack (see RESULTS AND DISCUSSION).

RESULTS AND DISCUSSION

In the following, we will illustrate the wall adaptation procedure for the typical flow case $M_\infty = 0.7$ and $\alpha = 7°$. The wing is in the high position, 3.25 inches above the tunnel centerline. A flow chart of the algorithm is presented in figure 3.

The first step is an assessment of the wall interference at the model position. Figures 4,5 and 6 show the induced Mach number and angle of attack at three spanwise locations with the tunnel walls set to aerodynamically straight. The blockage interference is small and constant at the wing planform. However, the induced upwash varies considerably, in chordwise as well as in spanwise direction. At the wing root, for example, $\Delta\alpha$ increases from 0.3° at the leading edge to 1.7° at the trailing edge. A similar behavior occurs at the location of the mean aerodynamic chord (figure 5) and the wing tip (figure 6).

Figure 7 summarizes the wall interference experienced by the model. This plot appears on the control monitor of the wind tunnel computer during the test. It indicates the progress of the adaptation and helps the researcher to position the target line for the wall shape calculation (equation 12). The calculated Mach number increment ΔM at each spanwise location simply is an average value across the respective chord. The lift interference across the span is represented by the induced <u>absolute</u> angle-of-attack (ref. 17):

$$\Delta\alpha_{abs}(Y) = -1/\pi \int_0^\pi \partial\phi_W/\partial Z(\Theta,Y,Z_0)(\cos\Theta-1)d\Theta \qquad (22)$$

In this way, the induced camber at each spanwise section is properly taken into account.

Interference is highest at the wing root and we position the target line accordingly. The wall interference assessment method then calculates the blockage and upwash along this line. In other words, the previously computed interference velocities at the selected wing location are extended upstream and downstream.

The next step is to determine improved wall shapes. It is possible to completely eliminate the blockage and lift interference at the target line. The necessary deflections are calculated in eq. (21). However, the required constant downward wall slope downstream of the model may result in jack movements beyond the 2-D design limits. It is therefore more practical to eliminate the upwash <u>gradient</u>. We simply achieve this by setting $s_0 = 0$ in (21), that is by ignoring the constant part in the induced upwash distribution. The resulting wall shape appears to be rotated about the anchor points compared with the 'fully' adapted contours. Figure 8 shows this schematically.

Figure 9 presents the actual wall contours after the first iteration. The largest deflection of about 0.65 inches occurs in the region of the model. These rather small displacements are quite feasible in a 2-D adaptive test section. For example, the 0.3-m adaptive wall test section allows a maximum jack movement of 3 inches upward and 1 inch downward.

The residual interference after the wall adjustment is shown in figure 10 for the wing root. The induced angle of attack is virtually constant across the chord, as expected. The remaining Mach number deviation is beyond measurement accuracy.

The upwash and blockage interference at the other spanwise locations is, of course, simultaneously reduced. Figure 11 summarizes the results.

However, the induced angle of attack still varies across the wing span. This residual spanwise gradient is an inevitable limitation of a 2-D wall adjustment (deflections constant across the tunnel width). In practise, we may need to reduce the span of the tested model to achieve the required accuracy. However, conclusions are difficult to draw at this point. The model aspect ratio will undoubtedly play an important role. Numerical simulations done by Smith provide some insight into this problem (ref. 18).

The remaining wall interference had no significant effect on the measured model data in this test. We can see this on figure 12 for $M_\infty = 0.7$ and the wing in the high position. The model lift measured with the flexible walls set to aerodynamically straight (fig. 9) is larger than the 7x10 (interference-free) values. However, a linear correction based on the induced angle-of-attack at the mean aerodynamic chord of the wing ($2y/b = 0.42$, see figure 7) is generally sufficient in this case. Only for the highest angle of attack, do we actually need to deflect the walls to achieve correctability. As expected, a second wall adjustment has little effect on the model measurements.

Figure 13 shows a similar comparison for the wing in the center position. Again, the model lift in the adapted test section agrees well with the interference-free data throughout the whole angle-of-attack range.

However, noticeable discrepancies remained for $M_\infty = 0.85$. Figure 14 presents the results obtained with the wing centered. Adapting the walls reduces the wing lift as it should, but not to the extent necessary to simulate free-air conditions. This defect may be partly caused by a Reynolds number mismatch ($Re = 1.5 \times 10^6$ compared with 0.73×10^6 in the 7x10 test, ref. 15). Another contributing factor undoubtedly was the inaccurate interference assessment due to an insufficient number of wall pressure orifices.

CONCLUDING REMARKS

Although a 2-D adaptive-wall test section cannot precisely simulate interference-free flow around a 3-D model, it can improve the correctability of the test data to a considerable extent. However, some residual spanwise variation of wall interference is inevitable. The required wall deflections are feasible within 2-D design limits.

ACKNOWLEDGMENT

The authors wish to thank the adaptive wall research team, headed by Edward J. Ray, for the outstanding support of the research project.

REFERENCES

1. Sears, W. R.: Self-Correcting Wind Tunnels. Calspan Report No. RK-5070-A-2, July 1973. Also: Aeronautical Journal, Vol 78, 1974.

2. Tuttle, M. H. , Mineck, R. E.: Adaptive Wall Wind Tunnels - A Selected, Annotated Bibliography. NASA TM 87639, August 1986.

3. Ganzer, U.: A Review of Adaptive Wall Wind Tunnels. Prog. Aerospace Sci., Vol. 22, pp. 81-111, 1985.

4. Sears, W. R. , Erickson, J. C.: Adaptive Wind Tunnels. Ann. Rev. Fluid Mech., Vol. 20, 1988.

5. Wolf, S. W. D, Ray, E. J.: Highlights of Experience with a Flexible Walled Test Section in the NASA Langley 0.3-Meter Transonic Cryogenic Tunnel. Paper 88-2036, presented at AIAA 15th Aerodynamic Testing Conference in San Diego, May 18-20, 1988.

6. Kemp, W. B.: Toward the Correctable-Interference Transonic Wind Tunnel. Paper presented at AIAA 9th Aerodynamic Testing Conference in Arlington, Texas, June 7-9, 1976.

7. Harney, D. J.: Three-Dimensional Testing in a Flexible-Wall Wind Tunnel. AIAA-Paper 84-0623.

8. Wedemeyer, E.: Wind Tunnel Testing of Three-Dimensional Models in Wind Tunnels with Two Adaptive Walls, VKI Preprint 1982-36, Sept. 1982.

9. Lamarche, L., Wedemeyer, E.: Two-dimensional Wall Adaptation for Three-dimensional Flows, VKI Preprint 1984-34, Sept. 1984.

10 Lamarche, L.: Reduction of Wall Interference for Three-dimensional Models with Two-dimensional Wall Adaptation. Ph.D. Thesis, University of Brussels, Dec. 1986.

11. Archambaud, J. P., Mignosi, A.: Two-Dimensional and Three-Dimensional Adaptation at the T2 Transonic Wind Tunnel of ONERA/CERT. Paper presented at AIAA 15th Aerodynamic Testing Conference in San Diego, May 18-20, 1988.

12. Rebstock, R.: Procedures for Computing Transonic Flows for Control of Adaptive Wind Tunnels. NASA TM-88530, Jan. 1987.

13. Powers, D. L.: Boundary Value Problems. Academic Press, New York 1972.

14. Press, W. H., Flannery, B. P., Teukolsky, S. A., Vetterling, W. T.: Numerical Recipes. Cambridge University Press 1986

15. Sleeman, W. C. Jr., Klevatt, P. L., Linsley, E. L.: Comparison of Transonic Characteristics of Lifting Wings from Experiments in a Small Slotted Tunnel and the Langley High-Speed 7- by 10- Foot Tunnel. NACA RM L51F14, 1951.

16. Mokry, M.: Subsonic Wall Interference Corrections for Half-Model Tests Using Sparse Wall Pressure Data. NAE Aeronautical Report LR-616, Nov. 1985.

17. Kuethe, A. M., Chow, C.: Foundations of Aerodynamics. Fourth Edition, John Wiley & Sons, 1986.

18. Smith, J.: A Theoretical Exploration of the Capabilities of 2-D Flexible Wall Test Sections for 3-D Testing. NLR Rep. MP 84018 U, Feb. 1984.

TABLE 1. Three-Dimensional Semispan Adaptation Test

- **Unswept wing model**

Aspect ratio	**4.0**
Taper ratio	**0.6**
Airfoil section	**NACA 65A006**
Semispan/width	**0.51**
Reference data	**LRC 7' x 10' tunnel - 1951**

- **Test conditions**

Mach number	**0.7 - 0.85**
Angle of attack	**0^o to 7^o**

- **Test configurations** — **Wing centered and high**
- **Measurements** — **Model forces; wall pressures and deflections**

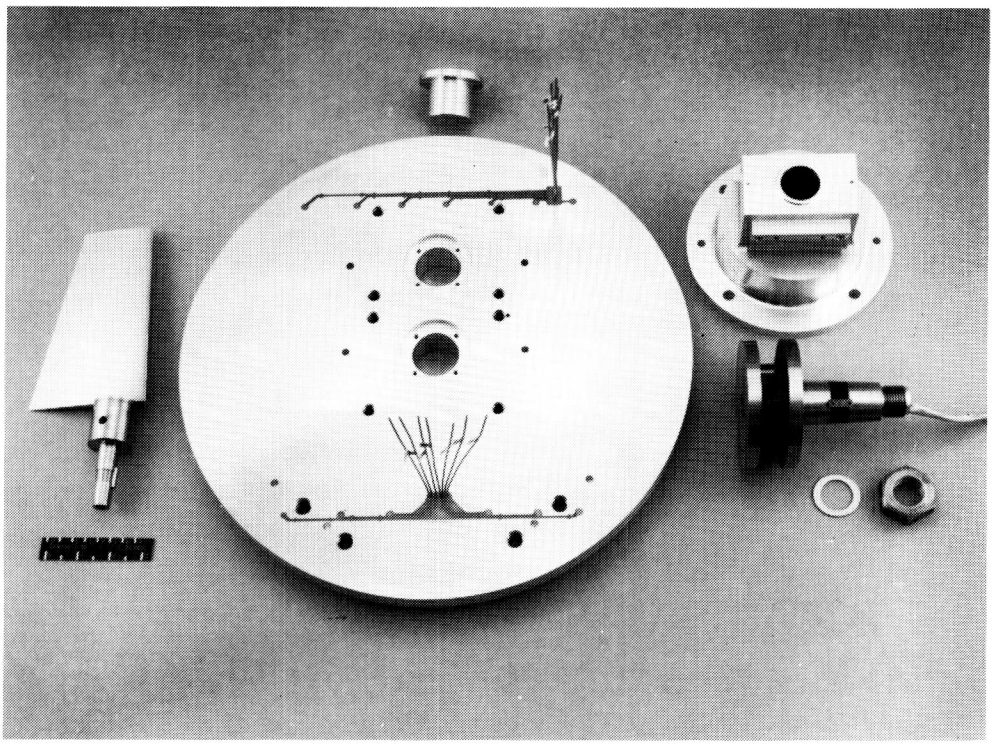

Figure 1. Semispan force-model apparatus.

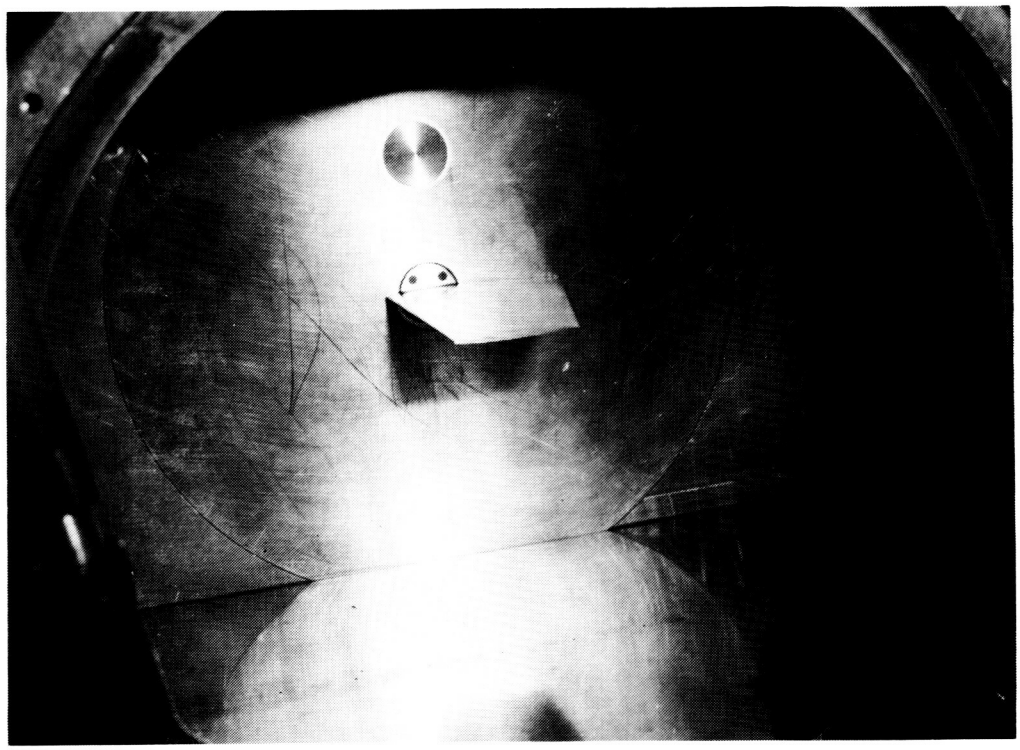

Figure 2. Model installed in Langley 0.3-m Transonic Cryogenic Tunnel.

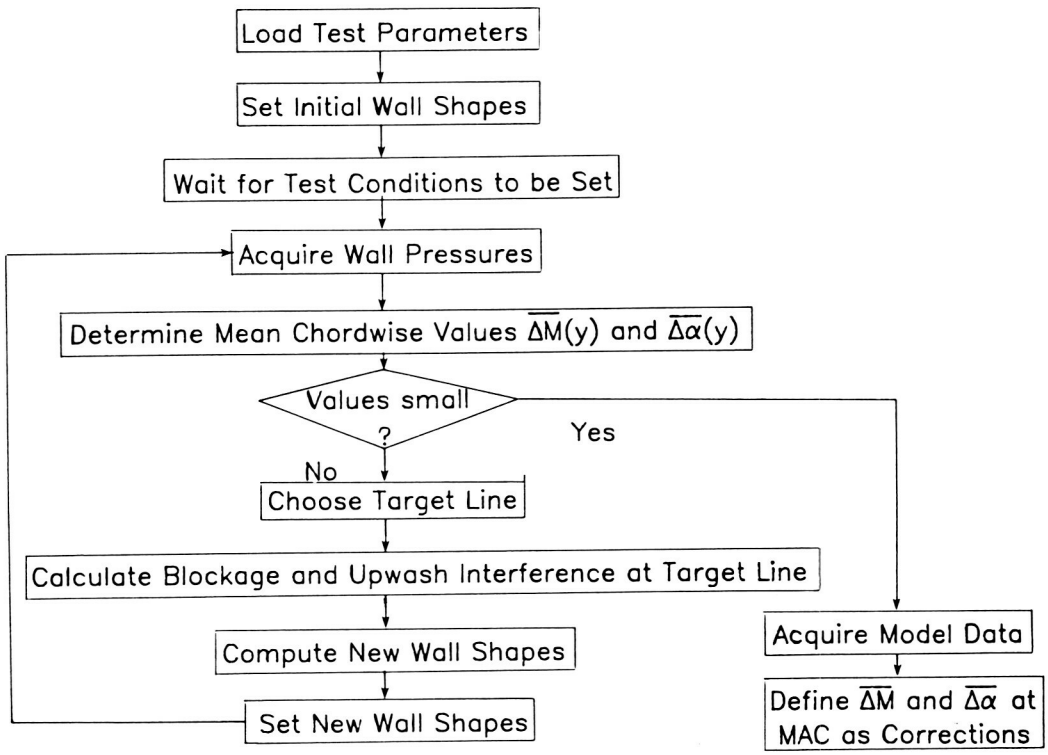

Figure 3. Wall adaptation flow chart.

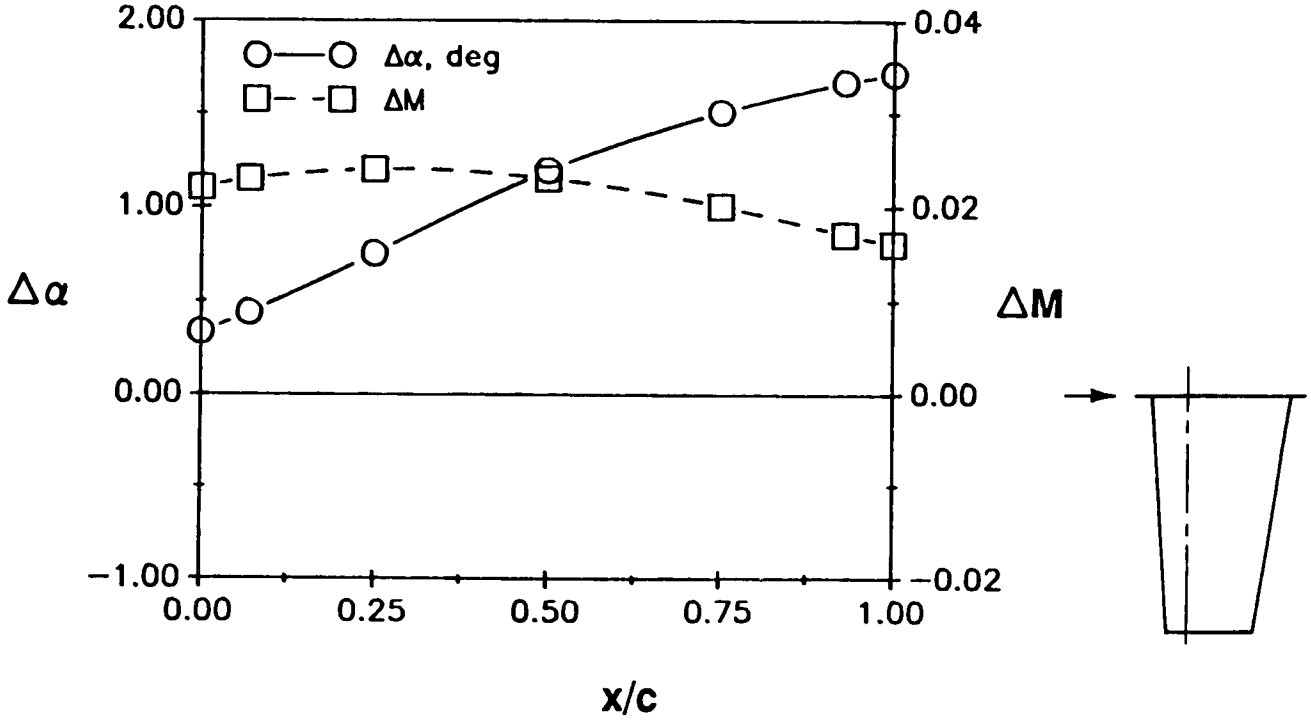

Figure 4. Chordwise variation of wall interference, walls straight, $M_\infty = 0.7$, $\alpha = 7^o$, wing high.

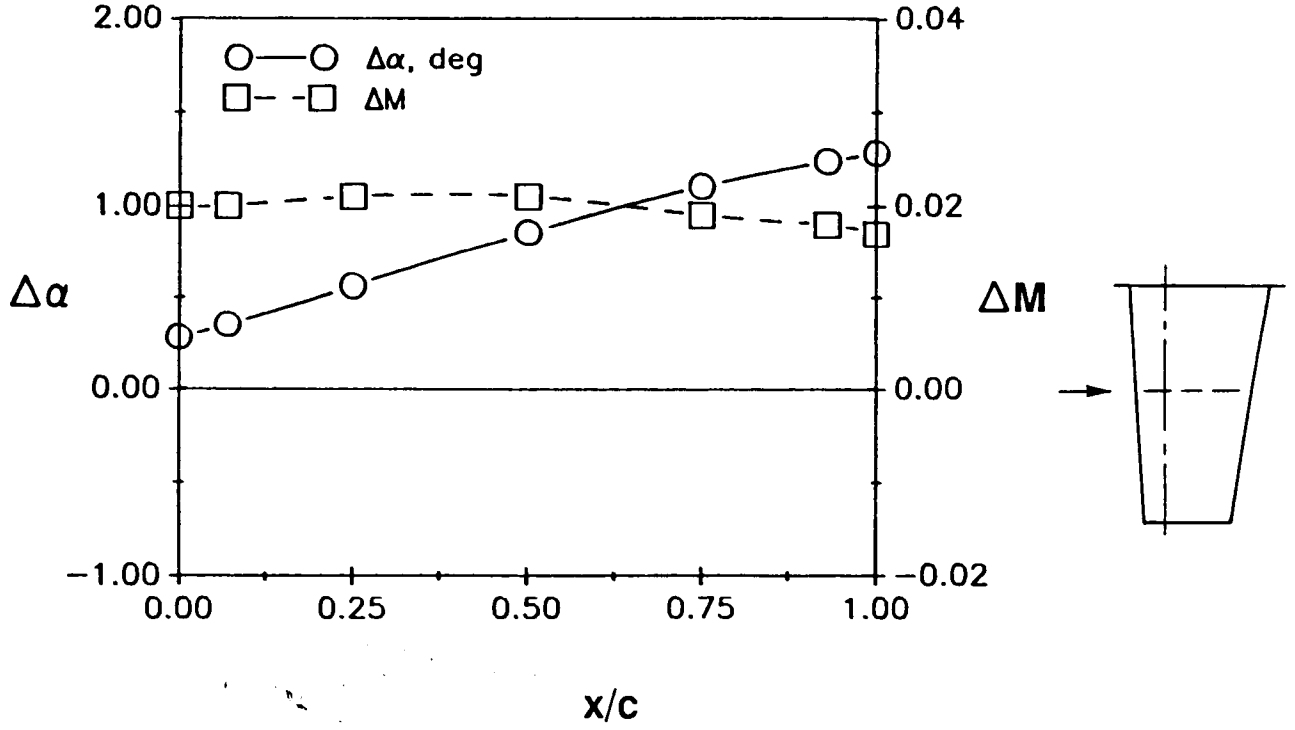

Figure 5. Chordwise variation of wall interference, walls straight, $M_\infty = 0.7$, $\alpha = 7^o$, wing high.

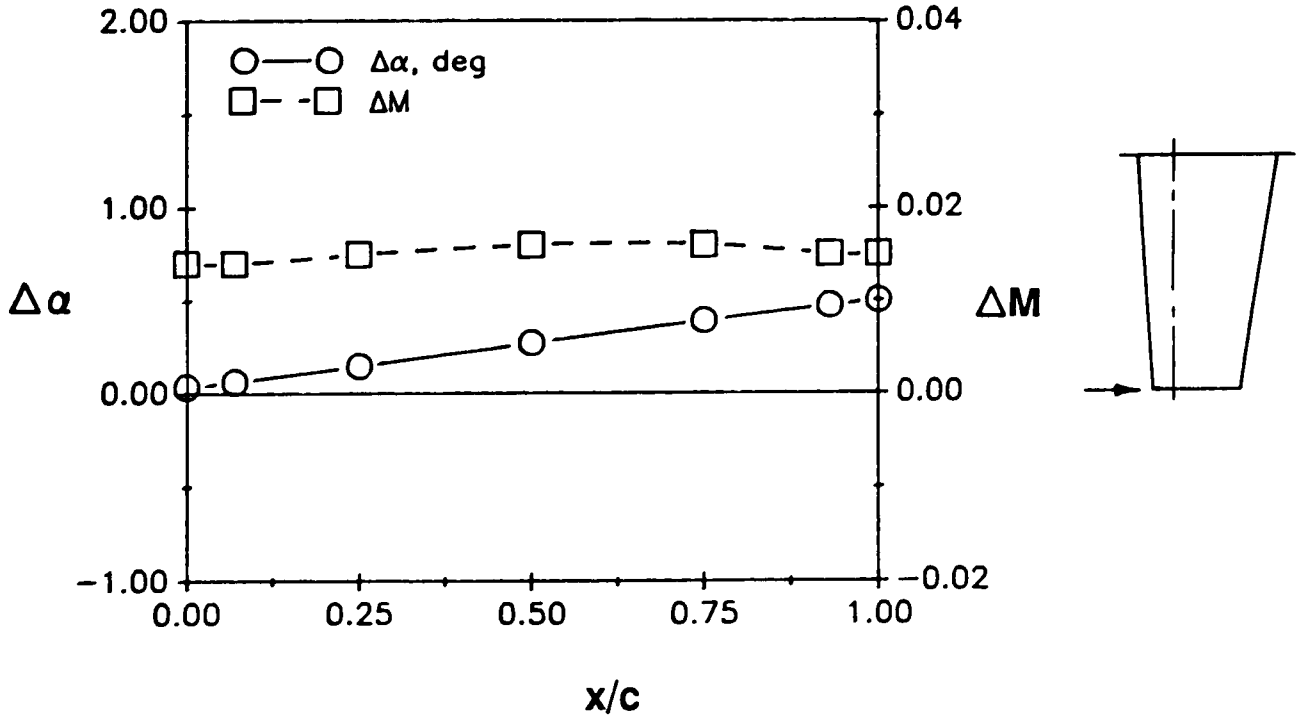

Figure 6. Chordwise variation of wall interference, walls straight, $M_\infty = 0.7$, $\alpha = 7^o$, wing high.

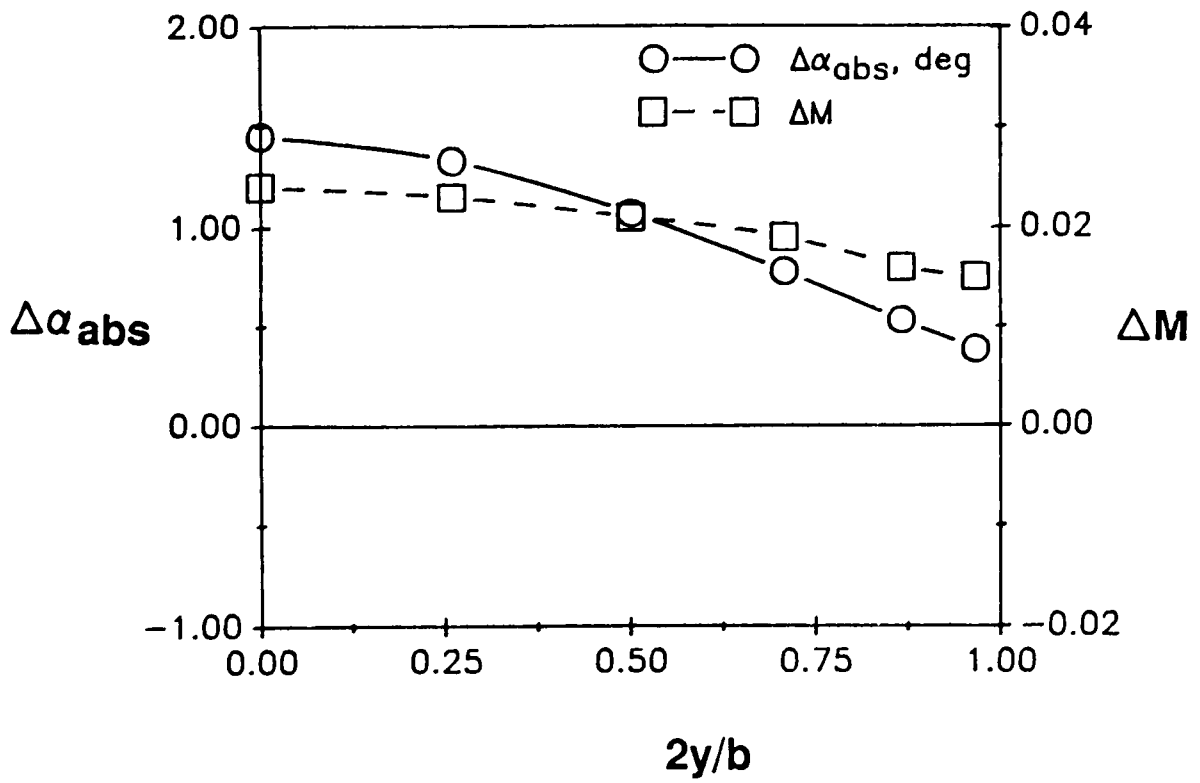

Figure 7. Summary of wall interference along the wing span, walls straight, $M_\infty = 0.7$, $\alpha = 7^o$, wing high.

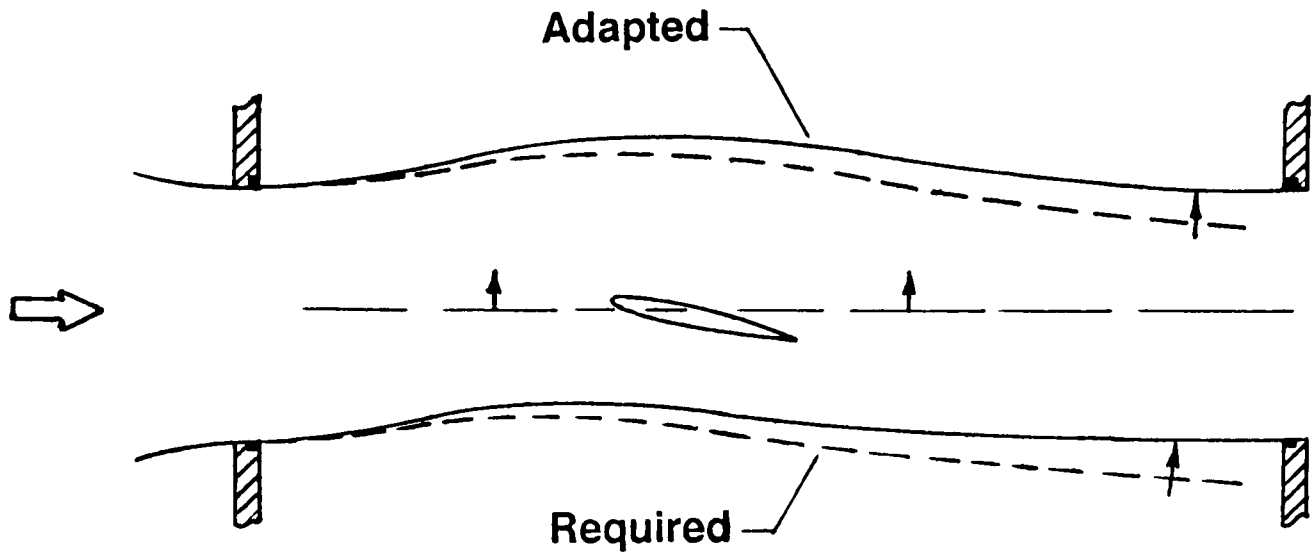

Figure 8. Flow field rotation.

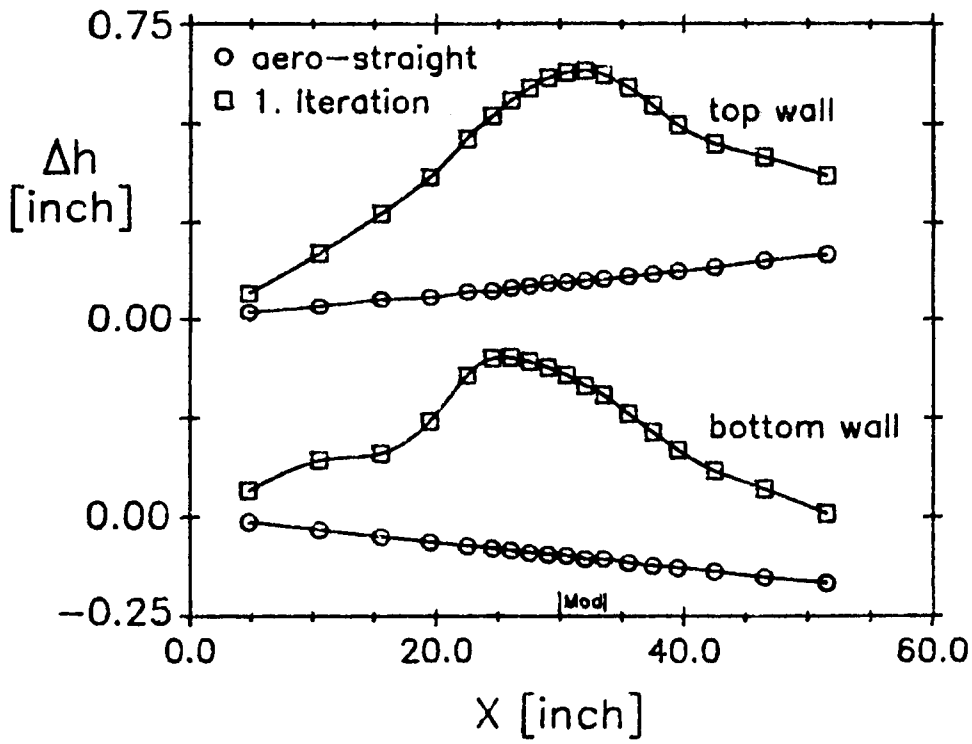

Figure 9. Wall deflections, $M_\infty = 0.7$, $\alpha = 7^\circ$, wing high.

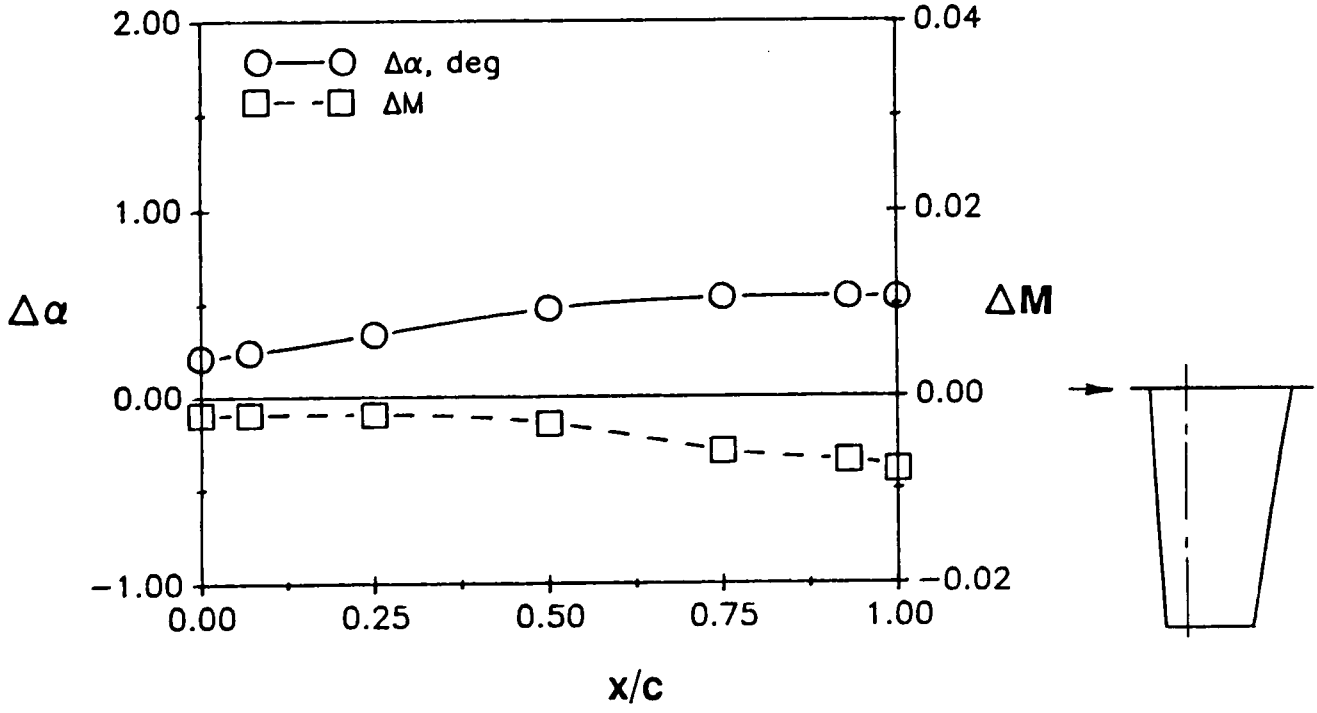

Figure 10. Chordwise variation of wall interference, first iteration, $M_\infty = 0.7$, $\alpha = 7^\circ$, wing high.

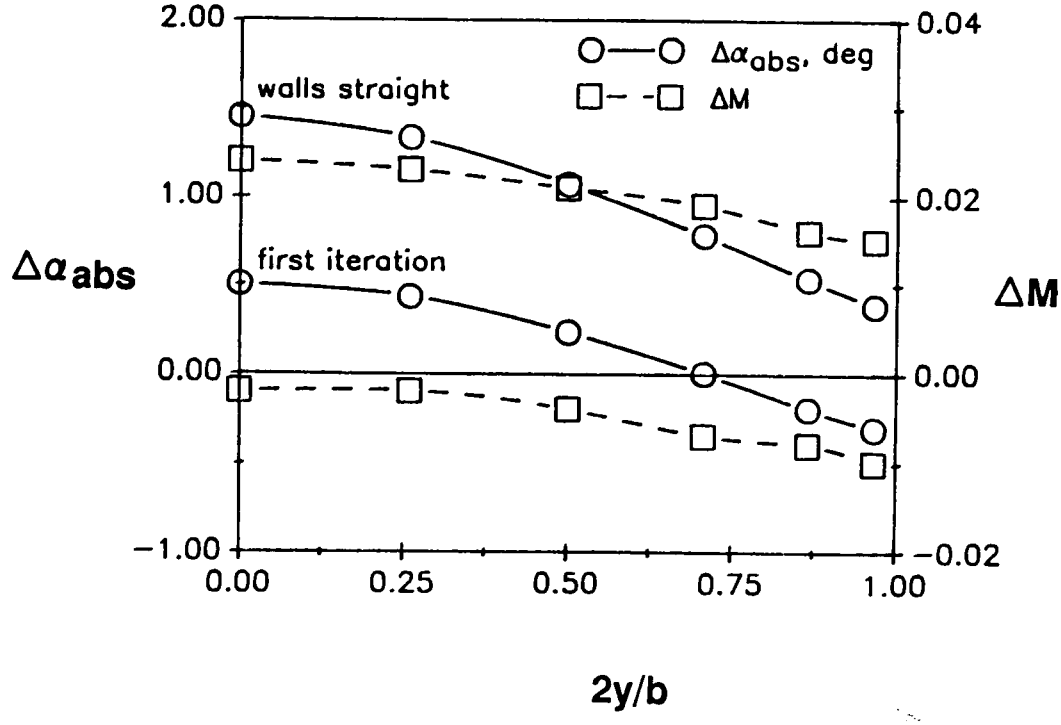

Figure 11. Interference at wing after first wall adjustment, $M_\infty = 0.7$, $\alpha = 7^\circ$, wing high.

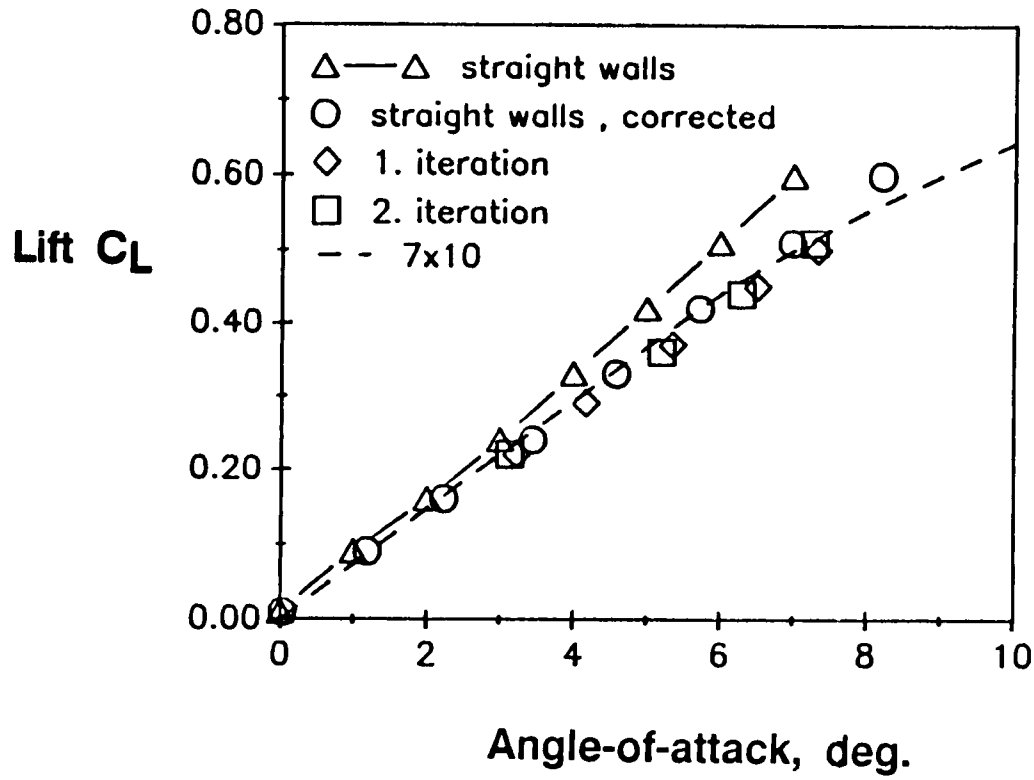

Figure 12. Measured wing lift versus interference-free data, $M_\infty = 0.7$, wing high.

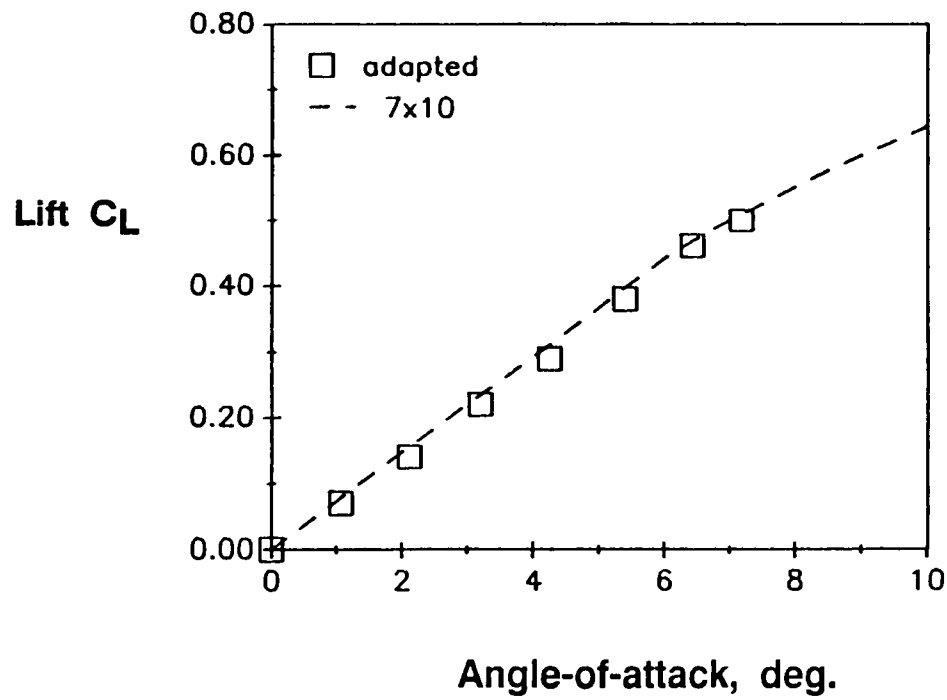

Figure 13. Measured wing lift versus interference-free data, $M_\infty = 0.7$, wing centered.

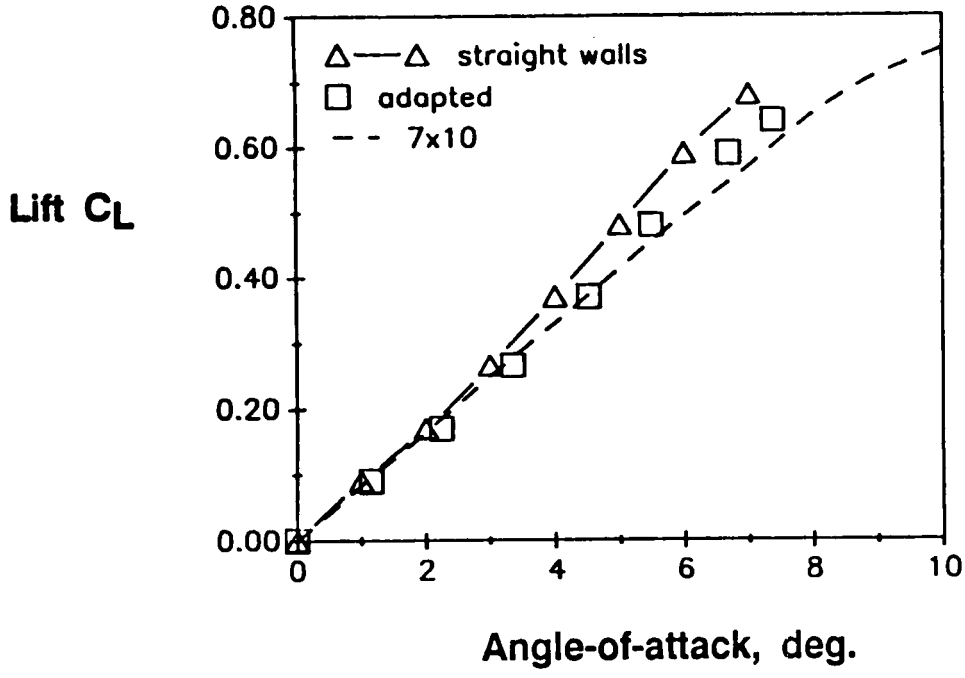

Figure 14. Measured wing lift versus interference-free data, $M_\infty = 0.85$, wing centered.